JOURNAL OF MATERIALS SCIENCE 20 (1985) 2133–2140

Mechanical and thermal response of shock-consolidated Mar-M 200 rapidly-solidified powder

MARC A. MEYERS, HAN-RYONG PAK
Center for Explosives Technology Research and Department of Metallurgical and Materials Engineering, New Mexico Institute of Mining and Technology, Socorro, New Mexico 87801, USA

Consolidation of rapidly solidified Mar-M 200 powder was carried out successfully using the axi-symmetric and plane-wave (using contact explosives with normal incidence) geometries. However, cracking produced by reflected waves remains a major problem and considerable development work will be required until it can be eliminated. The ambient temperature ultimate compressive strength of the consolidated powder is approximately 2200 MPa. The change in micro-indentation hardness and microstructure as a function of isochronal anneals of one hour between 600 and 1200° C are presented. Ageing compact to optimum hardness (850° C/1 h) raises the ultimate compressive strength to 2250 MPa.

1. Introduction

Rapid solidification technology seems to present a bright potential. One approach to consolidating rapidly-solidified powders is by the application of shock waves; preliminary results have indicated that it is feasible [1–3]. The consolidation of metal powders by explosives has been known for over twenty years and has been the subject of a number of investigations; Prummer [4] recently reviewed the field. Nevertheless, the process is still in its development stage; a recent study by the National Materials Advisory Board [5] highlights the potential and limitations of shock-wave consolidation. This paper describes the results obtained as a continuation of the exploratory investigative effort reported recently by Meyers *et al.* [3]. An additional consolidation geometry, plane wave by normal explosive detonation, was used, and some of the problems of explosive consolidation are presented. The mechanical strength (under compression) and the alteration of substructure of the consolidated powders with aging temperatures are reported.

2. Experimental techniques

The axi-symmetric consolidation system used in part of the experiments is described by Meyers *et al.* [3]. A plane-wave system using contact explosive (a cylinder of C-4) was also used; in this system the powder was inserted in a cavity machined into a mild steel cylindrical container. An aluminium punch was press-fit into the container after the powder was inserted. The container was evacuated by connecting a vacuum pump to an outlet. The pressure induced in the aluminium by the 62.5 mm thick C-4 plastic explosive was calculated to be 25 GPa.

Microhardness indentations were made by using a Tukkon apparatus at a load of 50 gf. The compression tests were carried out in a 89 kN MTS (Model 810) universal testing machine. The cylindrical specimens (length: 12 mm; diameter: 6 mm) were machined from the portion of the compact having the best characteristics and no central hole. They were placed between especially machined platens made of AISI 4140 steel hardened to HRC 55; castor oil was used as a lubricant between the platens and specimen. Substructural characterization by transmission electron microscopy was carried out in a Hitachi HU-200 electron microscope operated at 200 kV. Thin foils were prepared by the technique described in [3]. Aging was

0022–2461/85 $03.00 + .12

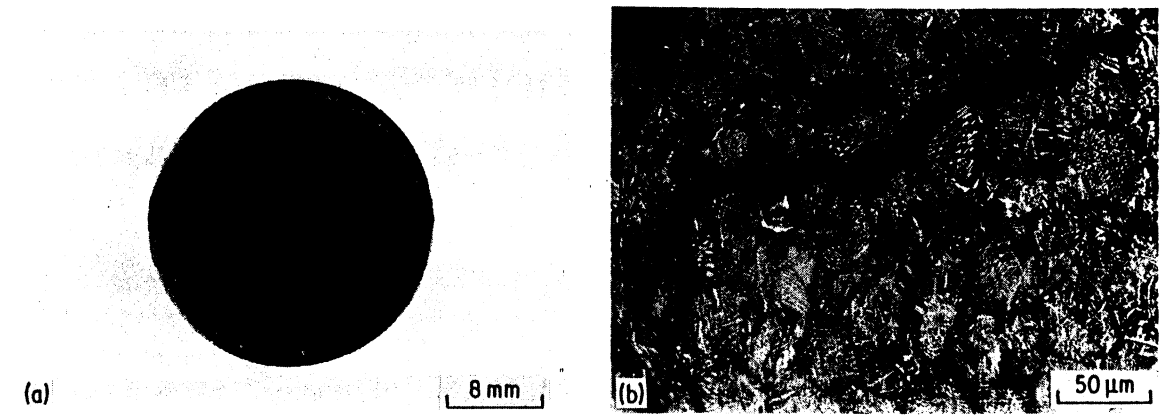

Figure 1 Cracks developed during consolidation using axi-symmetric system. (a) Radial and circumferential cracks. (b) Micrograph showing how cracks propagate in an interparticle mode.

carried out in a muffle furnace. The aging specimens were protected from oxidation by being packed in Sen/Pak heat treating containers. A Hitachi HHS-2R scanning electron microscope was used for the fractographs.

3. Results and discussion

It was possible to achieve good consolidation of the powders at E_m/T_m (explosive mass/tube mass) ratios of 10 [3], using the axi-symmetric geometry. This is the simplest configuration to produce shock-wave compaction, but presents inherent problems and limitations. The convergent shock waves reinforce themselves towards the centre; this is balanced by their attenuation. Upon continuing their outbound trajectory, they generate strong tensile stresses in the consolidated cylinder. This results in cracking, as evidenced by Fig. 1. Both radial and circumferential cracks were observed, and they seriously degrade the integrity of the consolidated cylinder. A closer observation after etching (Fig. 1b) showed that these cracks propagated in an interparticle mode. The elimination of cracking is possible, but would require exhaustive and systematic experimentation, once the system dimensions are chosen. Another limiting feature of this technique is the formation of a central hole above a critical E_m/T_m ratio; Fig. 2a shows longitudinal and transverse views of the central hole. This central hole is a well-known feature of axi-symmetric compaction. It has been attributed by Staver [6] to the formation of a Mach wave; recent computer simulations by Wilkins and Cline [7] have shown that it is due to a reversal of the material flow in the central region. Yust and Harris [8] also observed variations in the microstructure between the core and mid-radius position of explosively-consolidated

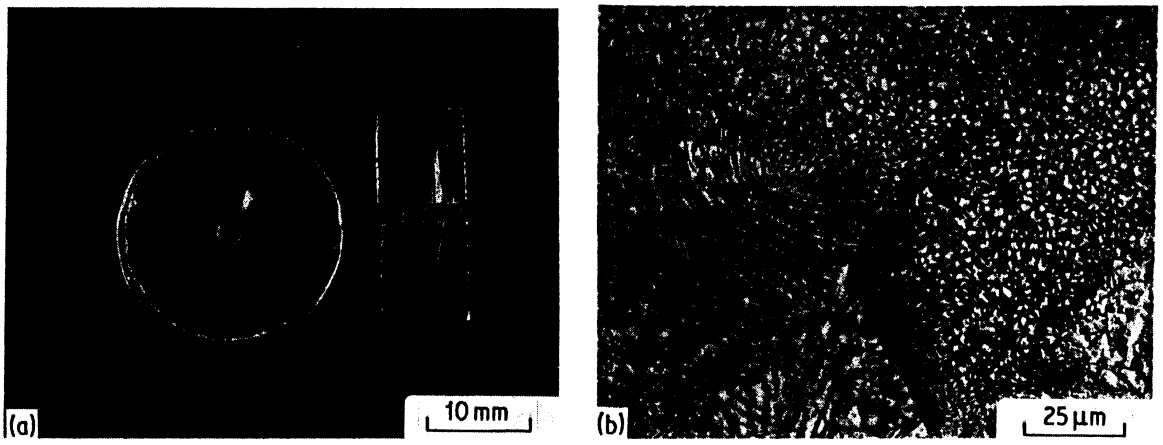

Figure 2 (a) Central hole in compact using axi-symmetric system. (b) Micrograph showing disappearance of dendritic structure in proximity of central hole (longitudinal section).

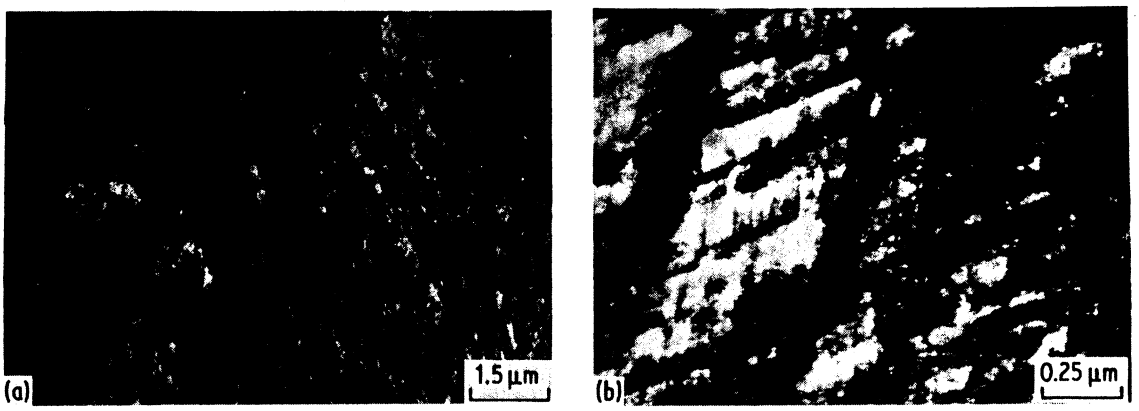

Figure 3 (a) Twinning and high dislocation banding observed by transmission electron microscopy. (b) Slip bands.

alumina. Evidence of intense heating is shown in the right-hand side of Fig. 2b; one clearly sees that the original microdendritic structure of the particles is replaced by equiaxed grains with approximately 2 μm in diameter, this region is adjacent to the hole. Hence, some kind of jetting phenomenon takes place, ejecting the powders from the centre. The central hole formation was observed for E_m/T_m above 10 and its diameter was found to be maximum (2 mm) for the highest E_m/T_m ratio used ($\sim$ 15).

The intitial structure of the powders consisted of microdendrites. Since the post-compaction substructure of the specimens consolidated by the axi-symmetric technique has been characterized before [3], only the plane-wave system is dicussed here. The substructure is identical to the one observed in the axi-symmetric system. The dendrites are distorted by the deformation process required to consolidate spherical particles into a three-dimensional body. Between the particles, and mainly at triple junctions, one observes white-etching regions, which are thought to be due to melting and rapid resolidification of the material; the melting is produced by the intense heat generation associated with the quasi-adiabatic deformation process. The rapid solidificaiton, generating a microcrystalline structure, is due to the intimate contact of the melt pools with large volumes (the inside of the particles) of metal with a temperature only slightly above room temperature. The existance of these interparticle melt regions has been recently confirmed by Morris [9] and Kasiraj *et al.* [10]; the results obtained by Morris [9] are in essence identical to those obtained by Meyers *et al.* [3].

One feature that rendered the analysis by transmission electron microscopy difficult is the extremely high dislocation density; individual dislocations could only be seen in certain regions. Fig. 3a shows the substructure characteristic of the particle interiors in the as-consolidated condition; the plane of the foil is close to (1 1 0). Heavy deformation is evidenced by the non-parallelism of the deformation twins; the angle between them in Fig. 3a is as large as 10°. Dense dislocation "patches" are seen on the left-hand side. Fig. 3b shows the appearance of a highly deformed central region at a higher magnification. Dislocation banding on two planes is clearly seen. This type of dislocation configuration is to be expected after shock loading [11, 12] superalloys.

As one approaches the boundaries between particles, more and more material flow is observed by optical microscopy; this can be seen by the distortion undergone by the dendrites (Fig. 1b). Fig. 4a shows the distortion as observed by transmission electron microscopy. The asterism of the diffraction spots is substantially increased, and the substructure is finely divided into subgrains in regions. The right-hand side of the micrograph shows the elongated grains in a convergent pattern. The grains could have been formed either by recrystallization occurring concurrently with deformation (dynamic recrystallization) or by melting and rapid resolidification. Gil Sevillano *et al.* [13] have recently reviewed deformation substructures at high strains and have described the transition from dislocation cells to subgrains at higher strains. When the misorientation between cells reaches a certain critical level, subgrains are formed; this can be seen by the more pronounced boundaries. Fig. 4b shows the boundary between two particles. Extensive material flow is clearly evident around the boundary (vertical line through centre of photomicrograph). This dark line has a

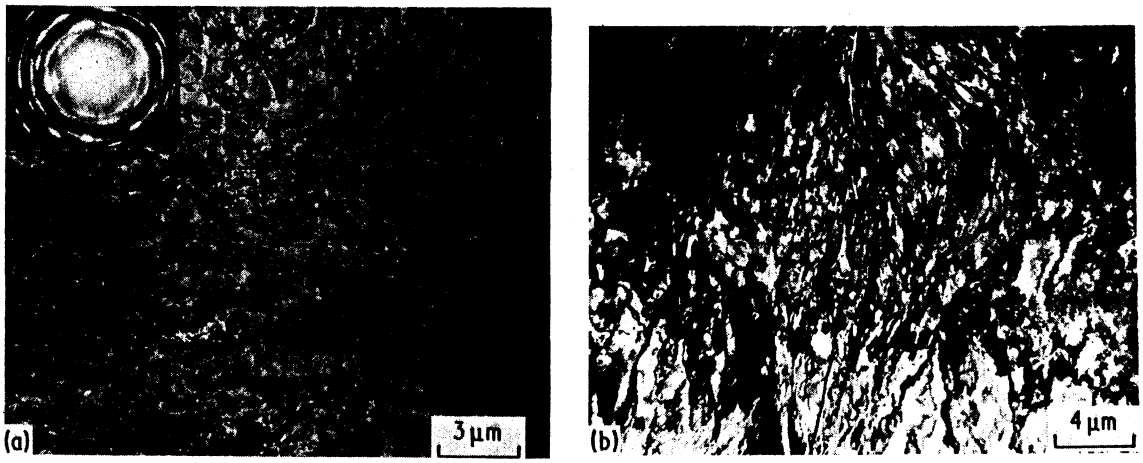

Figure 4 Substructure resulting from extensive material flow (and, perhaps, melting) (a) close to particle exterior and (b) at the interface between two particles.

well-defined thickness and could be due to an oxide layer originally surrounding the particles. They were exposed to air for prolonged periods prior to consolidation. Another hypothesis is that this layer is of metallic glass produced by melting and ultra-fast resolidification of the grain-boundary layer due to interparticle friction. One part of the boundary is clear; this could be due to (a) imperfect bonding or (b) etching of the particle boundary material.

The numerous cracks in the body of the material consolidated by the axi-symmetric technique precluded the preparation of tensile specimens. Hence, it was decided to prepare small cylindrical compression specimens of the end portion of the cylinder, which did not exhibit central hole or cracking due to a particularly favourable configuration of the compressive wave. The high ductility exhibited by the material on machining was evidenced by the long chips produced. This feature is very encouraging and demonstrates the intrinsic ductility of the consolidated material. Fig. 5 shows two compressive stress–strain curves for the as-shocked material (full and dashed lines); the curves show that the ultimate compressive strength of the material is approximately 2200 MPa, while its 0.2% offset yield stress is approximately 1950 MPa. The specimens failed in shear mode. The fractured surface was smeared out due to the compressive-shear forces, and it was not possible to observe any relevant features on it. However, a small portion of another specimen that had failed by tensile forces exhibited interesting features. One can see the individual particles in the scanning electron micrograph of Fig. 6; the interparticle regions show tearing and ductile failure signs, while other regions clearly evidence debonding of the particles. Hence, one has a mixed mode of fracture where the interparticle melt regions show actual fracture, while other regions simply show debonding. This shows that the interparticle bond strength is lower than the particle (powder) strength.

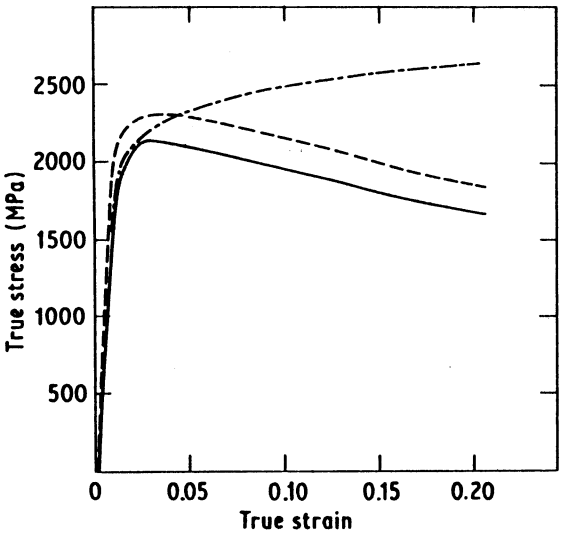

Figure 5 True stress – true strain curves for two specimens tested in compression; (——, - - - - -) as-consolidated; (— - — - —) after ageing 850° C for 1 h.

An interesting feature of the compressive curve is that it exhibits only limited work hardening. The maximum compressive strength is reached at a strain of 0.03 and the curve slopes downward after this. The observation of the polished and etched (transverse and longitudinal) sections of the

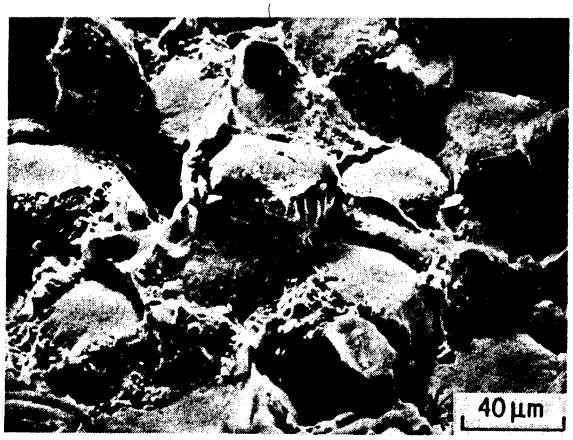

Figure 6 Appearance of tensile fracture region with tearing of interparticle melt regions.

compression specimens after rupture showed that the reason for the early loss of strength is the formation and growth of cracks. Numerous microcracks were observed throughout the specimen and their growth reduces the strength of the specimen. Fig. 7 shows the initiation and propagation or failure. Fig. 7a shows a void in the interparticle melt region acting as an initiation site for a microcrack. Numerous microcracks were found to nucleate in such interparticle melt regions. Fig. 7b shows several cracks growing between particles (see arrows); the interparticle mode is clearly evident. However, micro-indentation hardness measurements did not reveal any differences in hardness between the white regions and the microdendritic regions; hence, the initiation at these regions might be due to a lower ductility or to the presence of initiation sites and is not due to the lower strength. Fig. 7c shows a crack at a more advanced stage; one can, again, see that it follows the path dictated by the boundaries between particles.

The high level of strength achieved by shock-wave consolidation can be partially attributed to shock-wave strengthening. The dense deformation substructure generated increased the micro-indentation hardness of the particles from HV 400 to HV 720. This strengthening effect due to shock waves is well known. The other important factor is the inherent strength of the powders produced by rapid solidification processing; the high concentration of solid-solution elements in the matrix and the absence of massive carbides (crack-initiation sites) are the two principal reasons for the high intrinsic strength of these powders.

Since nickel-base superalloys derive a substantial portion of their strenth from precipitation, it was thought that the combination of shock-wave strengthening and aging would lead to an even higher strength. For this reason, 1 h ageing treatments were applied between 600 and 1200° C to observe the structural and mechanical property changes. Fig. 8 shows the variation of micro-indentation hardness. The hardness increases

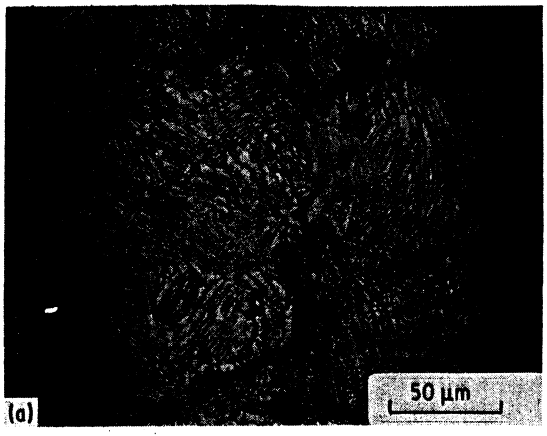

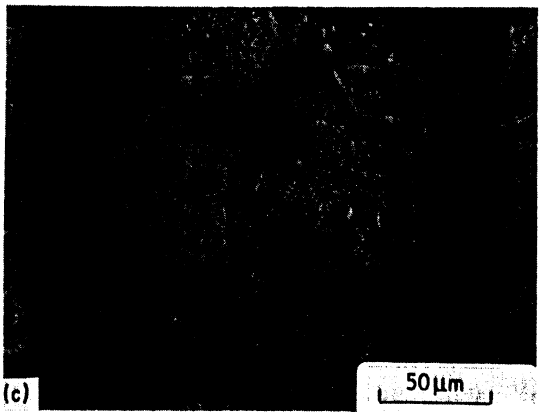

Figure 7 (a) Fracture initiation at void; (b) microcracks; (c) fracture.

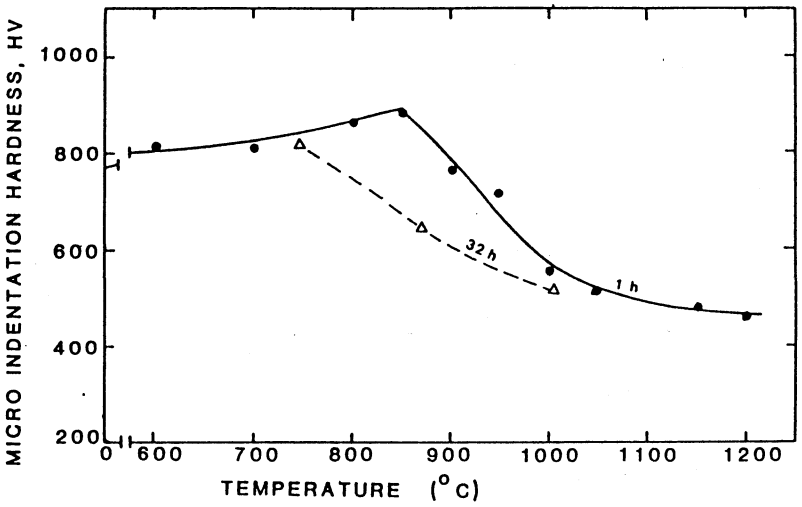

Figure 8 Effect of aging temperature on micro-indentation hardness of consolidated Mar-M 200.

steadily between 600 and 850° C, reaching its maximum of HV 875; at increasing temperatures, it drops again. The hardness after 32 h ageing treatments (commercial ageing time for Mar-M 200) at three different temperatures is also shown in Fig. 8. The hardnesses are lower than after 1 h treatments, and the ageing peak is shifted to a lower temperature. This reduction of the maximum hardness temperature for prolonged ageing times is expected, because more time is allowed for diffusional processes. The increase in microhardness (in comparison with the as-consolidated material) is clearly indicative of additional strengthening mechanisms operating.

A compression specimen was tested after ageing at 850° C for one hour (peak hardness) and the true stress-true strain curve is shown in Fig. 5. The added strength is evident, and one clearly sees the beneficial interaction between mechanical processing (shock-wave strengthening) and thermal processing (precipitation of gamma prime and carbides and dislocation reorganization). Although the yield stress is not cnanged, the ultimate compressive strength is increased to 2550 MPa and the material exhibits a substantial work-hardening range.

Transmission electron microscopy of the aged conditions revealed the changes in substructure as a function of temperature. Ageing at 600° C (Figs. 9 and 10) did not produce any observable change in substructure. Regions exhibiting deformation twins (Fig. 9) and regions showing dislocation arrays resembling patches (Fig. 10) could be observed. The electron diffraction pattern (Fig. 9a) and the dark field electron micrograph (Fig. 9b) identify the narrow black bands in Fig. 9a as the {1 1 1} microdeformation twins. After one hour at 800° C the dislocation substructure was not significantly alerted. Fig. 11a shows deformation twins superimposed on dense dislocation cell walls. (Although no twinning spots were observed in

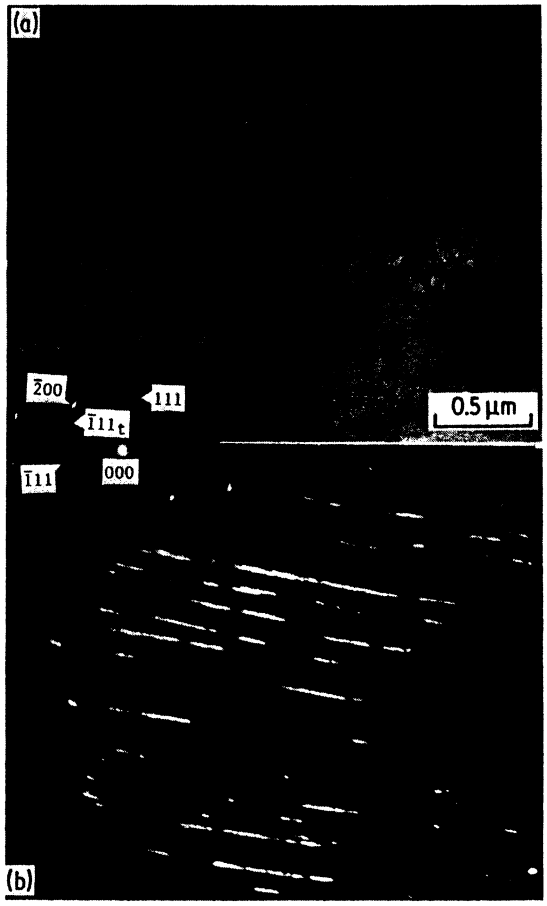

Figure 9 Substructure exhibiting deformation twins after aging consolidated alloy for one hour at 600° C; (a) bright field, (b) dark field of $\bar{1}\,1\,1_t$ reflection showing twins.

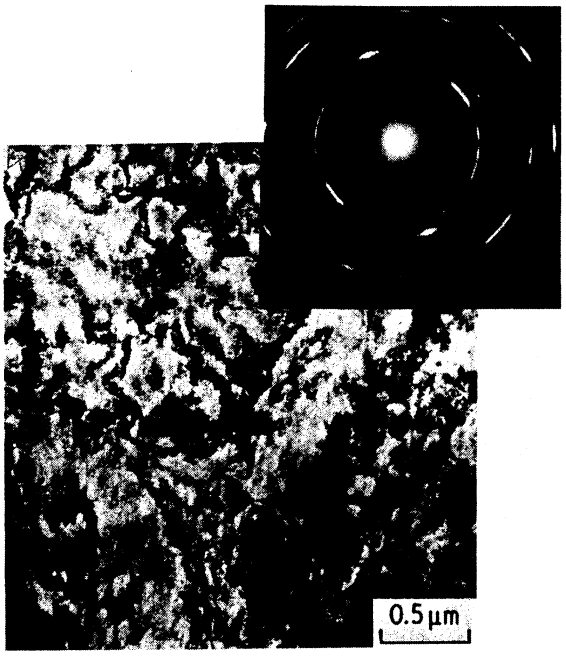

Figure 10 Substructure exhibiting dislocation patches after ageing consolidated alloy for 1 h at 600° C.

Fig. 11, narrow bands are thought to be {1 1 1} twins because the trace of these bands is parallel to (1 1 1) plane.) This temperature seems to produce the first noticeable precipitation activity. Fig. 11b shows small precipitates (indicated by arrow) along slip bands. These precipitates were not identified but are thought to be carbides. Gamma prime precipitation would produce a regular characteristic pattern which was not observed in Fig. 11. The small carbides seem to be responsible for the increased hardness of the alloy. The absence of massive gamma prime precipitation is in accord with Phillips [14] who noticed only a slight precipitation of material aged around 800° C for 1 to 24 h.

Ageing at higher temperatures for a period of 1 h resulted in gamma prime precipitates large enough to be viewed in the transmission electron microscope. The gamma prime precipitates were identified by the characteristic superlattice reflections resulting from Ni_3Al-type ordering observed in a foil obtained from the material aged at 1150° C. Fig. 12a shows the precipitation of gamma prime from the material aged at 950° C. The alignment of the precipitates along slip bands is evident; this type of configuration has been named "string of pearls" by Oblak *et al.* [15] The precipitates were found to be somewhat round in shape. The size of gamma prime precipitates increases with increase in ageing temperature, as seen by comparing Fig. 12b (material aged at 1150° C) with Fig. 12a. The gamma prime precitates not only increase in size but also change to the cuboidal shape. The same phenomenon was observed by Tewari [16].

4. Summary and conclusions

1. The ultimate compressive strength of the as shock-consolidated Mar-M 200 is approximately 2200 MPa. Ageing of the consolidated material at 850° C for 1 h (the temperature at which the hardness peaks) increases the ultimate compressive strength to 2500 MPa.

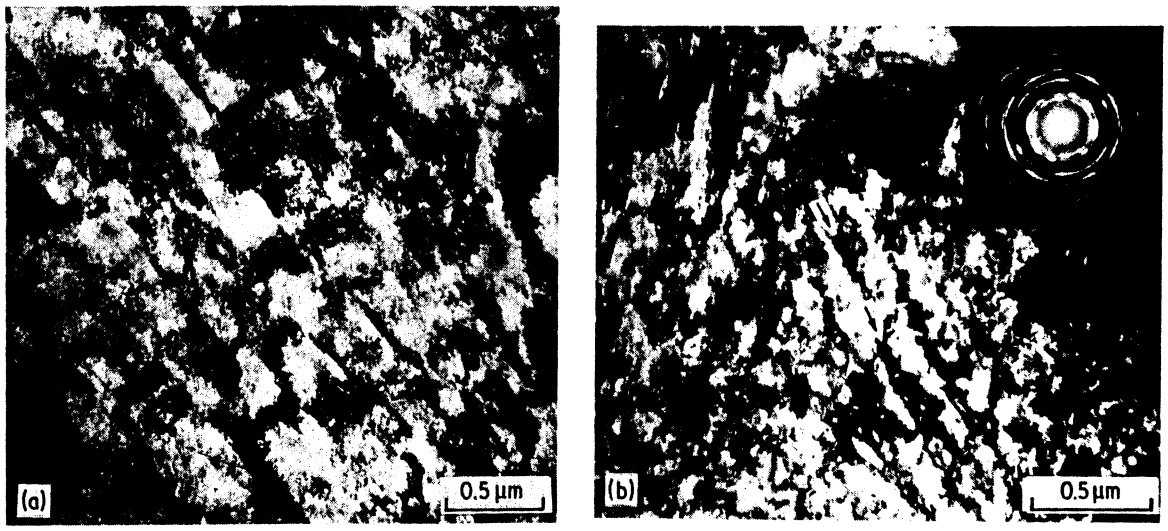

Figure 11 Substructures after ageing consolidated alloy at 800° C/1 h (a) Microtwins and dislocation patches; (b) evidence of precipitation along slip bands.

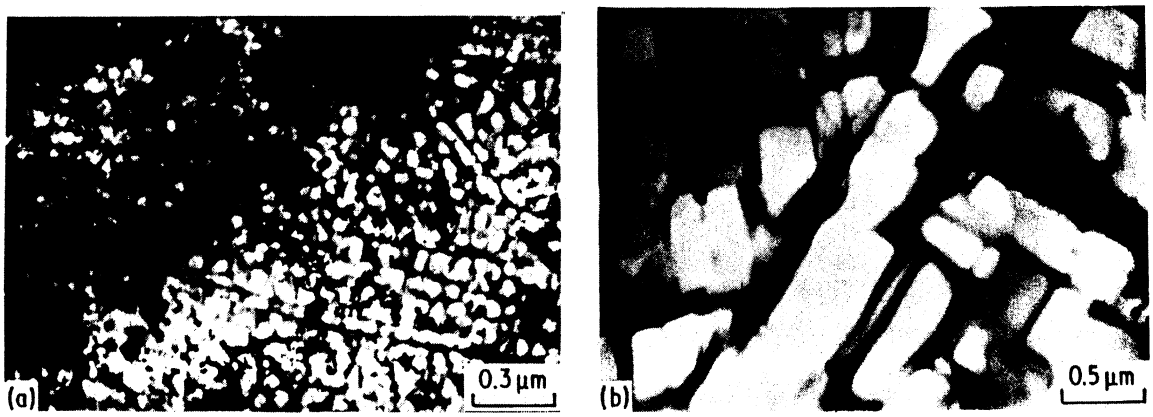

Figure 12 Gamma prime precipitates formed after ageing at (a) 950° C/1 h and (b) 1150° C/1 h observed by transmisssion electron microscopy.

2. The substructural features of the as-consolidated and the aged materials were observed by transmission electron microscopy. Twinning along {1 1 1} and profuse dislocations arranged in bands and "patches" were characteristic of the as-consolidated material. After ageing at 800° C/1 h, precipitation of carbides could be observed; aging at higher temperatures eliminated the deformation substructure and resulted in gamma prime precipitation.

Acknowledgements

The research was supported by NSF grant DMR 81 15127, by the Research and Development Division of New Mexico Tech, and by departmental funds graciously made available by Dr G. Purcell. The help of Mr B. B. Gupta and Mr S.-L. Wang in the preparation of the systems and of Mrs K. Couch-Robino in transmission electron microscopy is gratefully acknowledged. The Mar-M200 was kindly provided by Mr A. R. Cox, Pratt and Whitney Government Products Division.

References

1. C. F. CLINE and R. W. HOPPER, *Scripta Metall.* **11** (1977) 1137.
2. D. RAYBOULD, *J. Mater. Sci.* **16** (1981) 589.
3. M. A. MEYERS, B. B. GUPTA and L. E. MURR, *J. Met.* **33** (1981) 21.
4. R. A. PRUMMER, in "Explosive Welding, Forming and Compaction", edited by T. Z. Blazynski (Applied Science, London, 1982) Chap. 10, p. 369.
5. V. D. LINSE (ed.), "Dynamic Compaction of Metal and Ceramic Powders", NMAB-394 (National Academy Press, Washington, DC, 1983).
6. A. M. STAVER, in "Shock Waves and High-Strain-Rate Phenomena in Metals: Concepts and Applications", edited by M. A. Meyers and L. E. Murr (Plenum, New York, 1981) p. 865.
7. M. L. WILKINS and C. F. CLINE, "Simulation of Explosive Compaction Experiments", Proceedings of the Explosive Fabrication Conference Soviet Academy of Sciences, Novoskibirsk, USSR, September, 1981, p. 166.
8. C. S. YUST and L. A. HARRIS, in "Shock Waves and High-Strain-Rate Phenomenon in Metals: Concepts and Applications", edited by M. A. Meyers and L. E. Murr (Plenum, New York, 1981) p. 881.
9. D. G. MORRIS, *Mater. Sci. Eng.* 58 (1983) 187.
10. P. KASIRAJ, T. VREELAND Jr, R. B. SCHWARZ and T. J. AHRENS, in "Shock Waves in Condensed Matter", edited by J. R. Asay, R. A. Graham and G. K. Stranb (North Holland, Amsterdam, 1984) p. 439.
11. R. N. ORAVA, "Response of Nickel-Base Superalloys to Thermomechanical Processing by Shock-Wave Deformation", DRI–U. of Denver, Report No. DRI-2638, US Naval Air Systems Command (1979).
12. M. A. MEYERS and R. N. ORAVA, *Met. Trans.* **7A** (1976) 179.
13. J. GIL SEVILLANO, P. VAN HOUTTE and E. AERNOUDT, *Prog. Mater. Sci.* **25** (1980) 69.
14. V. A. PHILLIPS, *Acta Metall.* **14** (1966) 1533.
15. J. M. OBLAK, W. A. OWKZARSKI and B. H. KEAR, *ibid.* **19** (1971) 355.
16. S. N. TEWARI, *Met. Trans.* **7A** (1976) 1237.

Received 16 July
and accepted 31 July 1984